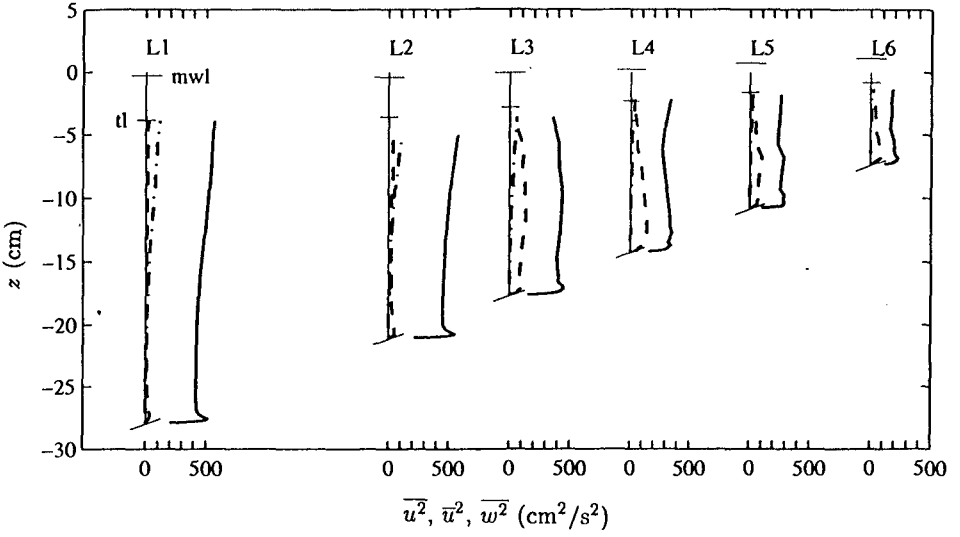

Figure 2: Vertical variation of $\overline{u^2}$ (——), $\overline{u}^2$ (– –), and $\overline{w^2}$ (–·–) for L1–L6.

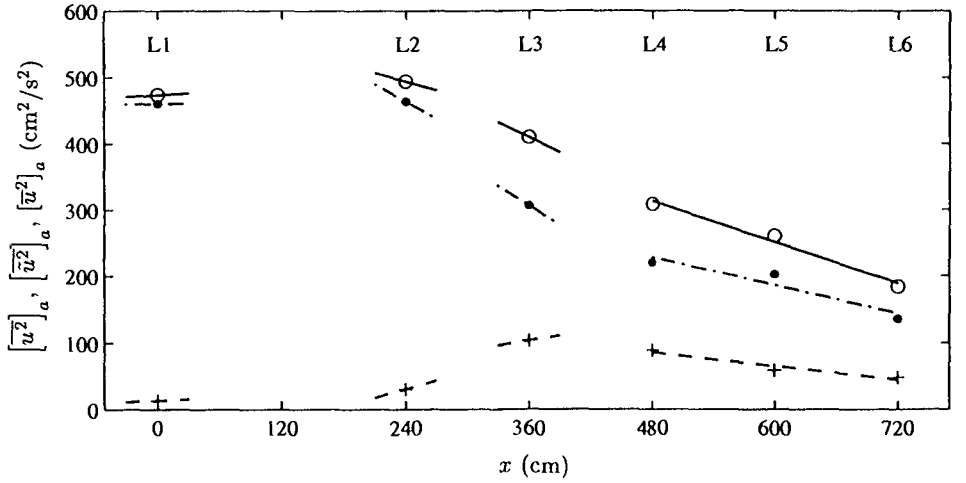

Figure 3: Cross-shore variation of $\left[\overline{u^2}\right]_a$ (○ ——), $\left[\overline{\overline{u}^2}\right]_a$ (• –·–), and $\left[\overline{u}^2\right]_a$ (+ – –) with gradients for L1–L6.

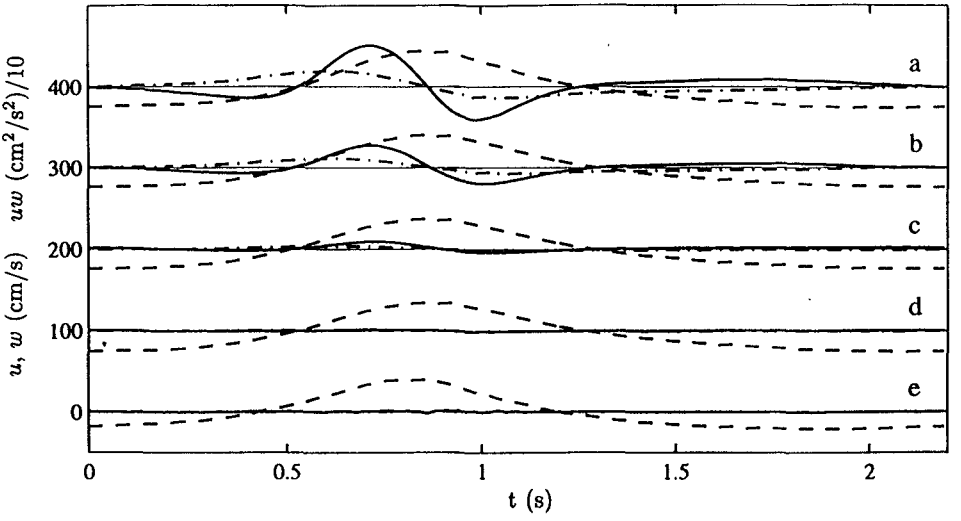

Figure 4: Temporal variation of u (– –), w (–·–), and uw (——) at five elevations for L1. To facilitate plotting, uw is reduced by a factor of 10, and there is an offset of a factor of 100 in the ordinate.

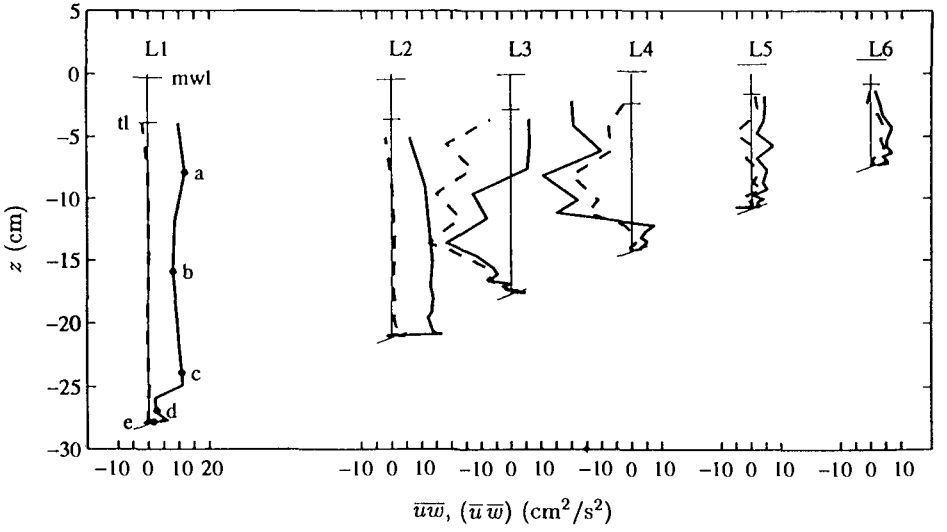

Figure 5: Vertical variation of $\overline{uw}$ (——) and $(\overline{u}\,\overline{w})$ (– –), for L1–L6. Five elevations of Fig. 4 at L1 indicated by solid circle (•).

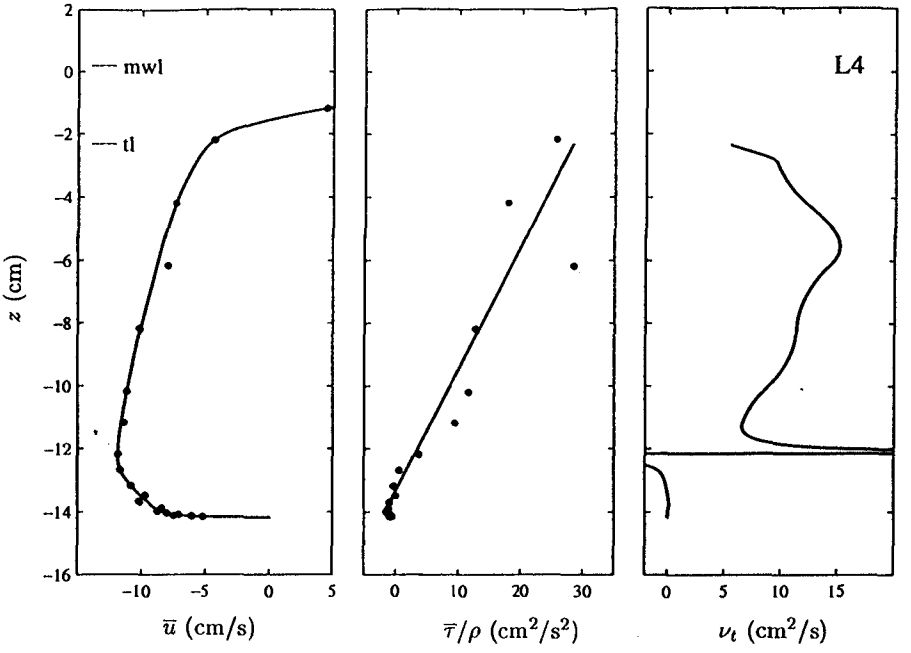

Figure 6: Vertical variation of measured $\overline{u}$ (•) with cubic spline (——) (left); measured shear stress $\overline{\tau}/\rho$ (•) with best-fit curve (——) (middle); kinematic viscosity ν_t (——) (right) for L4.

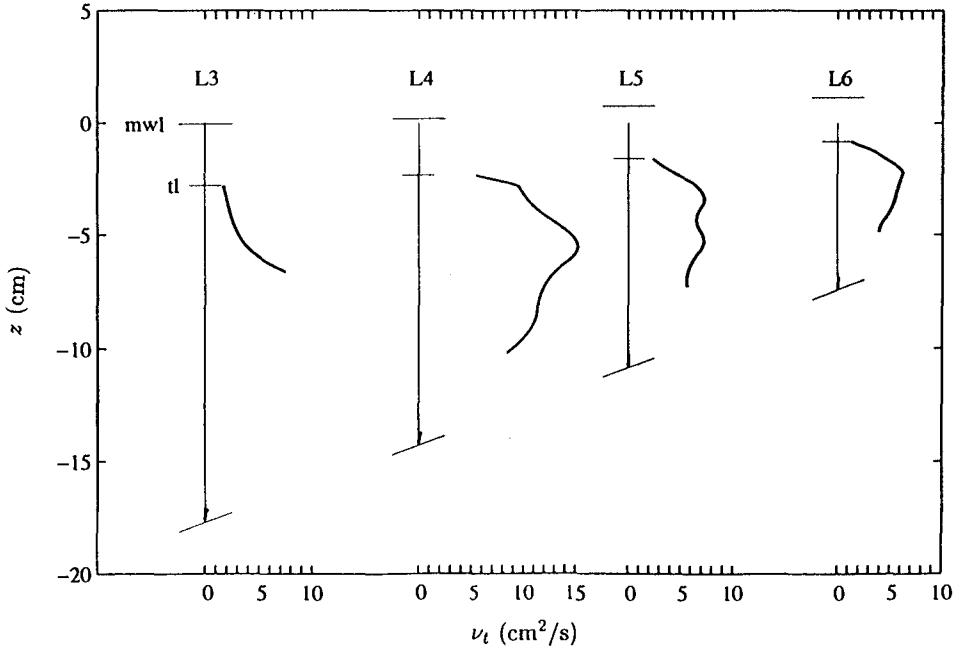

Figure 7: Vertical variation of measured eddy viscosity ν_t (——) for L3 to L6.

CHAPTER 248

A Comparison of Field Observations and Quasi-Steady Linear Shear Instabilities of the Wave Bottom Boundary Layer

D. L. Foster[1], A. J. Bowen[1], R. A. Beach[2] and R.A. Holman[2]

Abstract:

Field observations of near-bed high frequency velocity fluctuations and suspended sediment are compared with predictions of momentary flow stability by a quasi-steady linear instability model. Field observations were made as part of the Duck94 cooperative field experiment and consisted of a vertical array of four hot-film anemometers and 19 fiber-optic backscatter sensors located within the wave bottom boundary layer. Predicted instabilities for the quasi-steady model occur over length scales ranging from 2 cm to 1 m and therefore may be assumed to be a plausible mechanism for the generation of turbulence and suspension of sediment. However with the quasi-steady model, the instabilities are at the same phase as the sediment suspension events, but are occuring too late in the wave phase for them to be generating the observed turbulence.

[1] Department of Oceanography, Dalhousie University,Halifax, Nova Scotia, Canada, B3H 4J1.
internet: diane.foster@dal.ca

[2] Department of Oceanography, Oregon State University, Ocean Admin Bldg 104, Corvallis, Oregon, USA 97331.

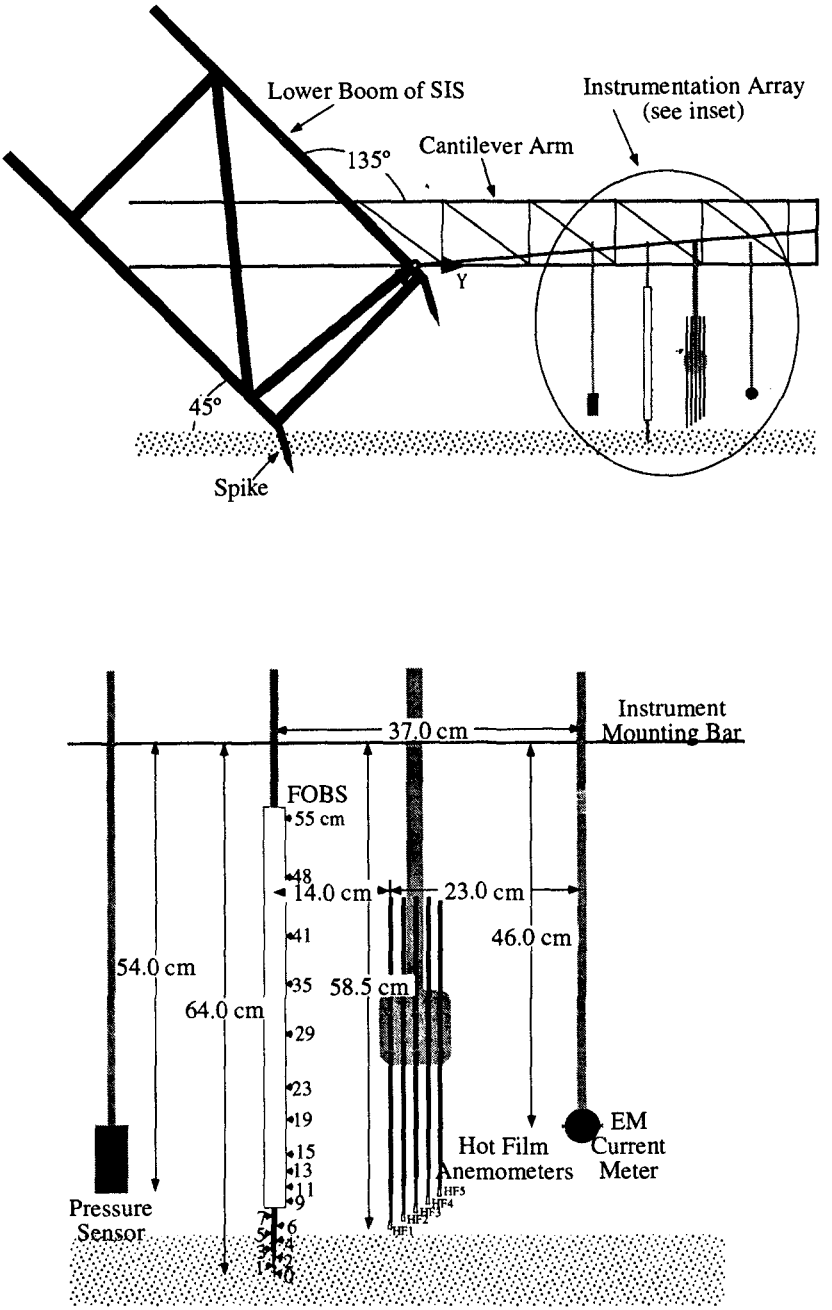

Figure 1: A schematic showing the instrument cantilever as deployed from the Sensor Insertion Sytem on the FRF pier(top panel) and positions of the pressure sensor, FOBS probe, hot film anemometer array, and electromagnitic current meter (bottom panel) (Foster, et al., 1996).

1 Introduction

The seemingly random occurrence of sediment suspension events in the surf zone has long been the topic of research for coastal oceanographers and engineers. These short-lived events are the first step in morphologic evolution and consequently hold significance in our understanding of coastal dynamics. Intuition suggests that suspension events are a result of rapid increases of turbulence levels in the near-bed region. The wave bottom boundary layer is the region of fluid bounding the seabed which responds to the oscillatory surface waves. Within this relatively small region ($\delta \sim$ O(5 cm)), the velocity transitions from the free stream value (u $\sim$ O(100 cm/s)) to zero. Thus far, most of the previous research on the introduction of turbulence to the wave bottom boundary layer has focussed on bottom shear generation. An additional and equally plausible mechanism is the generation of turbulence from within the wave bottom boundary layer through a shear instability. Using a piecewise continuous linear instability model, Foster, et al. (1994) showed that at particular wave phases, the high shears in this region may lead to shear instabilities. With laboratory observations of oscillatory boundary layer flow, Hino et al. (1983) concluded that increased levels of turbulence during the decelerating phase of the flow were triggered by a shear instability.

The objective of this paper is to compare Duck94 field observations of near-bed high frequency velocity fluctuations and suspended sediment with predictions of momentary flow stability by a quasi-steady linear instability model. This paper is organized in the following manner. An overview of the field experiment and data collection technique is given in section 2. The theoretical formulation and solution method of the shear instability problem is presented in section 3. Comparisons between the theory and observations are made in section 4. Finally, the conclusions are given in section 5.

2 Observations

The experiment was conducted at the Army Corps of Engineers, Field Research Facility (FRF) in Duck, NC (Figure 1) on August 17, 1994, as part of the Duck94 field experiment. The significant offshore wave height, angle, and period measured in 8 m water depth were 0.83 m, 50 from the southeast, and 4.54 s, respectively. The observations were made in 2 m water depth on the crest of the bar over flat bed conditions. The instruments were deployed from a cantilever arm attached to the lower boom of the sensor insertion system on the FRF pier, see Figure 1. Near bed velocity observations were made with an array of 5 hot-film anemometers, sampled at 256 Hz, separated with a 1 cm vertical spacing, Figure 1. The velocity outside the wave bottom boundary layer was measured with an electromagnetic current meter. The bed elevation and suspended sediment were measured with a vertical stack of 19 fiber-optic backscatter sensor probe (FOBS), sampled at 16 Hz. The bed elevation is determined by examining each independent sensor for burial. A thorough presentation of field techniques and instrument calibration may be found in Foster et al. (1996).

3 Theoretical Formulation

As formulated in Foster, et al. (1994), let the total velocity be partitioned into perturbation and wave components and given by

$$\begin{aligned} u^T(x,z,t) &= u(x,z,t) + U(z,t) \\ w^T(x,z,t) &= w(x,z,t), \end{aligned} \tag{1}$$

where x and z are the horizontal coordinates (x being positive offshore from the shoreline and z being positive up from the seabed), t is time, u and w are the perturbation velocities, and U is the known horizontal oscillatory background velocity. In a linear instability analysis, it is assumed that perturbation velocities are significantly smaller than the background velocity, simply $u, w << U$. Substituting (1) into the continuity equation, subtracting the linearized wave bottom boundary layer equation and neglecting terms of $O(u^2)$, we obtain the governing equation:

$$\begin{aligned} u_t + Uu_x + wU_z &= -\frac{1}{\rho}P_x + \nu(u_{xx} + u_{zz}) \\ w_t + Uw_x &= -\frac{1}{\rho}P_z + \nu(w_{xx} + w_{zz}), \end{aligned} \tag{2}$$

where P is the pressure and ν is the kinematic viscosity. By assuming conservation of mass and two-dimensional flow, it is possible to represent u and w in terms of the stream function, Ψ, such that

$$\begin{aligned} u &= \Psi_z \\ w &= -\Psi_x. \end{aligned} \tag{3}$$

Substitute the stream function definitions into (2), cross differentiate, and subtract to eliminate the pressure reducing to one equation

$$\left(\frac{\partial}{\partial t} + U\frac{\partial}{\partial x} + \nu\nabla^2\right)\left(\nabla^2\Psi\right) - U_{zz}\Psi = 0. \tag{4}$$

For this investigation, we neglect the effect of viscosity.

The quasi-steady model assumes that the time-varying background profile may be represented with a series of time-independent profiles, such that $U(z,t) \equiv U_n(z)$. At each instant in time, t_n, we assume a solution of the form

$$\Psi_n(x,z,t_n) = \phi_n(z)e^{i(k_n x - \sigma_n t_n)} \tag{5}$$

where k is the real wavenumber and $\sigma = \sigma_r + i\sigma_i$ is the complex frequency. The substitution of (5) into (4) results in the well known Rayleigh equation

$$(U_n - c_n)\left(\phi_{n_{zz}} - {k_n}^2\phi_n\right) = U_{n_{zz}}\phi_n. \tag{6}$$

The boundary conditions are specified by assuming that there is no mass flow through the bottom and that the perturbation must decay as $z \Rightarrow H$, where H is the water depth, and

are given by

$$\begin{aligned} \phi(z = z_o) &= 0 \\ \phi_z(z = \delta) &= -k\phi(z = \delta). \end{aligned} \tag{7}$$

(6) may be solved with a finite centered difference approximation scheme. For this model, we assume that the background flow may be approximated with a time- and depth-dependent eddy viscosity model (Foster, 1996).The wave bottom boundary layer background flow model was forced with a 256 second record of velocity measured at 13 cm above the bed. The system is discretized into 100 nodal points and solved numerically as an eigenvalue problem (Dodd, et al., 1992), where the wave celerity, $c = \sigma/k$, is the eigenvalue and the stream function, Ψ, is the eigenfunction.. The momentary flow stability is examined by searching for the fastest growing mode at each instant in time over a given wavenumber range of interest.

The concept of momentary stability (Shen, 1961) implies that when $\sigma_i > 0$ the disturbances are growing relative to the background flow and the flow may be considered to be "momentarily unstable". Conversely, when $\sigma_i < 0$ the disturbances are decaying relative to the background flow and the flow may be considered to be "momentarily stable".

4 Results

Flow stability was determined at 1/8 second intervals using the eddy viscosity model-generated background velocity profile, $U(z,t)$. An example of this can be seen in Figure 2. Notice that at times a and d the flow is stable and that at times b and c, when the free stream flow is decelerating and there exists an infection point in the profile, the flow is unstable. The peak growth rate occurs prior to flow reversal when the near-bed internal shear is largest. The oscillatory perturbation frequency, σ_r, is nearly zero in the two unstable cases, b and c, indicating that there will exist a fixed spatial pattern which grows exponentially in time. This may be a possible explanation for ephemeral ripples which form over a wave phase following a suspension event. An example of the eigenfunction amplitude and phase structures for 3 wavenumbers is given in Figure 3. For cases b and c, the peak phase shift is as large as $\pi/2$.

A 60 second time series of near bed cross shore velocity, turbulent variance, concentration, and predicted growth rates is given in Figure 4. The perturbation growth rates, concentration, and turbulent variance all have 'event-like' structures. Although instabilities are predicted during each 1/2 wave and more often than concentration or turbulent variance events, the larger perturbation growth rates are correlated to the highly correlated concentration and turbulent variance events. The concentration (increasing with increasing proximity to the bed) and turbulent variance (decreasing with increasing proximity to the bed) magnitudes vary over the vertical (Foster, 1996), however the temporal event-like structure is uniform throughout this near-bed region. For further comparisons, we use one FOBS sensor located at 3 cm above the bed and the vertically averaged turbulent variance.

To examine the evolution of the growth rates, concentration, and turbulent variance

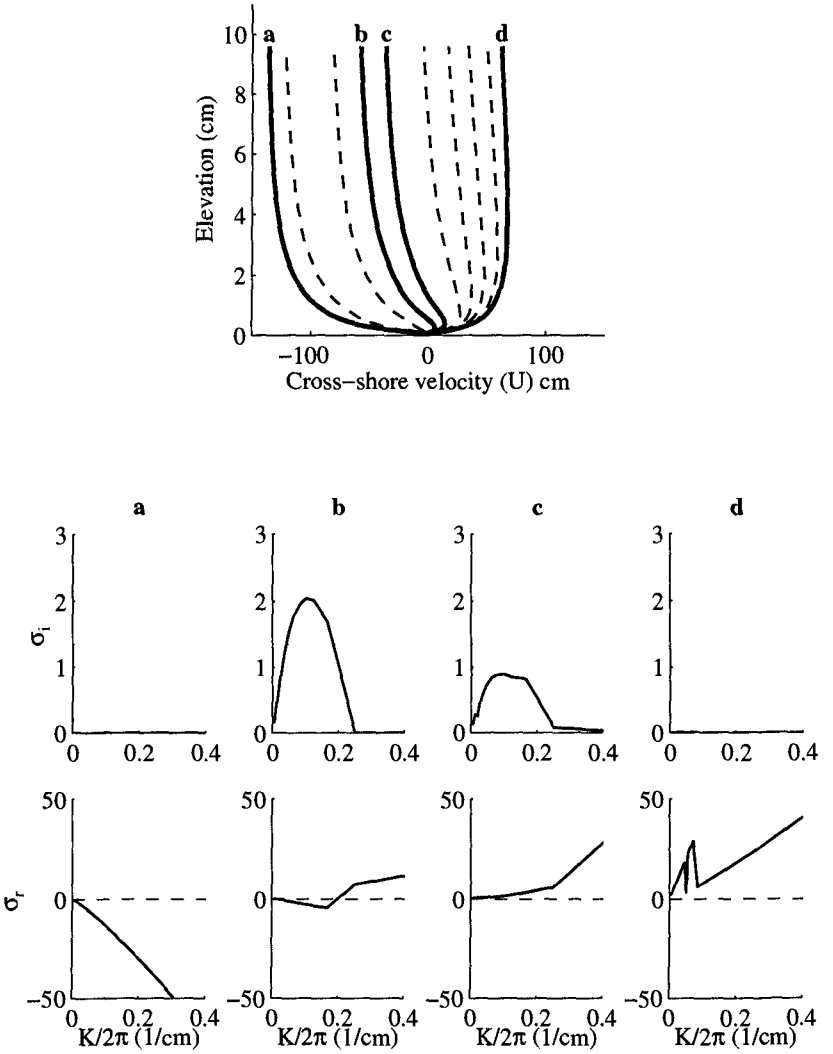

Figure 2: The top panels shows the vertical structure of $U(z,t)$ at 1/4 sec intervals over a 2.5 second record. At 4 of these times, a-d, we have shown the predicted perturbation growth rates, $\sigma_i(k)$ (Hz) (middle panels), and the real frequencies, $\sigma_r(k)$ (Hz) (bottom panels).

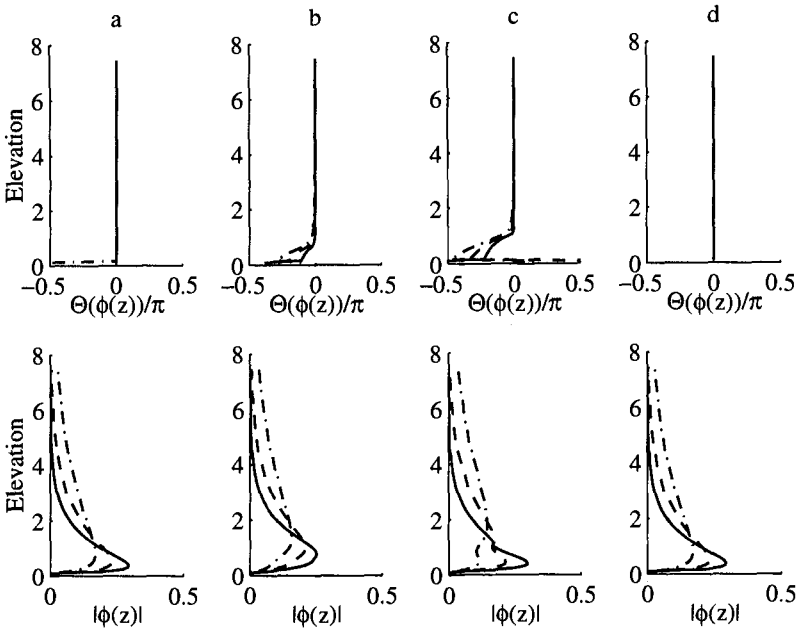

Figure 3: The top panels show the eigenfunction phase, $\Theta\phi(z)$, and the bottom panels show the amplitude, $|\phi(z)|$, for each of the 4 cases (a-d) for 3 selected wavelengths (straight line, 4 cm; dashed line, 10 cm; and dashed-dotted line, 20 cm).

over the course of the wave, we use a phase space averaging (PSA) technique. The PSA technique averages quantities of similar velocity and accelerations bins over a 256 second record. The acceleration is determined in the frequency domain with a tapered 1 Hz low pass cutoff frequency. This technique allows us to evaluate the phase averaged temporal event structure as it corresponds to the magnitude and phase of the background wave. The PSA for the growth rates, concentration, and turbulent variance are given in Figures 5, 6, and 7, respectively. The growth rate PSA shows two peaks, one prior to each of the flow reversal on the larger waves (the outer part of the wave ellipse), with the largest peak occuring after the wave crest when the internal shears are largest. The concentration PSA shows one peak during the flow reversal period following the wave crest prior to flow reversal at relatively the same phase as the growth rate. This peak also occurs at the outer part of the wave ellipse, indicating, not surprisingly, that concentration events are closely associated with the larger waves. The second peak in the concentration PSA occurs following the flow reversal and may be a result of the sediment plumes being advected back through the instrument array. The turbulent variance PSA shows a peak intensity at and following the large wave crest, leading to the concentration and predicted growth rates peaks. This indicates that the turbulence is occuring too early in the wave phase for it to a result from the instabilities predicted here.